frontiers | Frontiers in Astronomy and Space Sciences

TYPE Original Research
PUBLISHED 15 November 2022
DOI 10.3389/fspas.2022.1059242

OPEN ACCESS

EDITED BY
Jianguo Yan,
Wuhan University, China

REVIEWED BY
Zhen Zhong,
Guizhou Normal University, China
Xin Ren,
National Astronomical Observatories (CAS), China

*CORRESPONDENCE
Jinhai Zhang,
zjh@mail.iggcas.ac.cn

SPECIALTY SECTION
This article was submitted to Planetary Science, a section of the journal Frontiers in Astronomy and Space Sciences

RECEIVED 01 October 2022
ACCEPTED 02 November 2022
PUBLISHED 15 November 2022

CITATION
Zhang L and Zhang J (2022), Observation-based temperature field simulation at Zhurong landing site, Mars. *Front. Astron. Space Sci.* 9:1059242. doi: 10.3389/fspas.2022.1059242

Observation-based temperature field simulation at Zhurong landing site, Mars

Lei Zhang[1,2,3,4] and Jinhai Zhang[1,2,3,4]*

[1]Engineering Laboratory for Deep Resources Equipment and Technology, Institute of Geology and Geophysics, Chinese Academy of Sciences, Beijing, China, [2]Key Laboratory of Earth and Planetary Physics, Institute of Geology and Geophysics, Chinese Academy of Sciences, Beijing, China, [3]Innovation Academy for Earth Science, Chinese Academy of Sciences, Beijing, China, [4]College of Earth and Planetary Sciences, University of Chinese Academy of Sciences, Beijing, China

Modeling the temperature field near the Martian surface is critical for many scientific exploration tasks, such as detecting liquid water and analyzing the existence of saline ice. Meteorological conditions on Mars are highly dramatic, with a daily temperature change of up to 80–100 K. Most previous tasks of surface temperature monitoring on Mars are based on satellite observations, lacking *in-situ* measured data. Recently, two Martian missions at mid-low latitudes in the northern hemisphere, InSight lander and Zhurong rover, carried out near-surface temperature observations. However, the temperature monitoring of the Zhurong rover obtained data for only some short periods in its working days; thus, the amount of recorded temperature data is inadequate for a whole-day analysis at the landing site. Here we reconstruct the near-surface temperature at the Zhurong landing site by incorporating the continuous temperature data observed at the InSight lander, simultaneously referring to the Martian Climate Database; then, the reconstructed data are used to constrain the numerical simulation of the response of shallow subsurface under the Zhurong landing site. The numerical simulation of heat conduction shows that the daily temperature change under the Zhurong landing site mainly influences the uppermost depth of 0–30 cm, with a daily average temperature of ~225 K. During the traveling duration of the Zhurong rover (i.e., summer of Mars), the seasonal temperature change within the top 1 m is significant and is related to the thermal properties of possible subsurface media (e.g., soil, ice, and sandstones). Although there might be aqueous activities in Utopia Planitia, our results show that from the perspective of temperature field, there is little possibility of liquid water in the shallow subsurface under the Zhurong landing site. The proposed method in this study provides a new way for the temperature field simulation of the subsurface in areas with insufficient local observations, especially on extraterrestrial objects.

KEYWORDS

Mars, temperature, subsurface, Zhurong rover, Tianwen-1 mission

Introduction

China's Zhurong rover successfully landed on Mars in 2021, at southern Utopia Planitia (Zhou et al., 2020; Wu et al., 2021; Ye et al., 2021; Zhao et al., 2021; Niu et al., 2022), where is thought to have been an ancient ocean. Having experienced complex ancient geological events (Acuna et al., 1999; Zhong and Zuber, 2001; Stanley et al., 2008; Christensen et al., 2009; Zhang et al., 2022a), the present meteorological condition on Mars is still extreme. The Zhurong landing site is in the mid-low latitude (25.066° N), with four distinct seasons. There are significant differences in wind speed and direction in different seasons (Charalambous et al., 2021; Gou et al., 2022). The air pressure changes steadily as the revolution process on Mars (Banfield et al., 2020). According to wind conditions during different seasons, an entire martian year can be divided into dust-storm season (mainly autumn and winter in the northern hemisphere) and quiet season (mainly spring and summer in the northern hemisphere).

The daily temperature difference of the near-surface is extremely large (up to 80–100 K) and varies significantly with seasons. The large temperature variation strongly affects the near-surface and subsurface meteorologic conditions (Banfield et al., 2020) and even the thermal behavior of the lander on Mars (Zhang et al., 2023a). The temperature field and its seasonal variation in the subsurface layer of Zhurong landing area are very important for water/ice detection. Previous studies have conducted thermal simulations on a seasonal timescale (Li et al., 2022) for evaluating the temperature field in the subsurface based on Martian Climate Database (MCD, Forget et al., 1999). For *in-situ* observation-based thermal simulation, the problem is that only a short period of temperature data was collected by Zhurong during its working days; thus, the amount of recorded temperature data is inadequate for a whole-day analysis at the landing site.

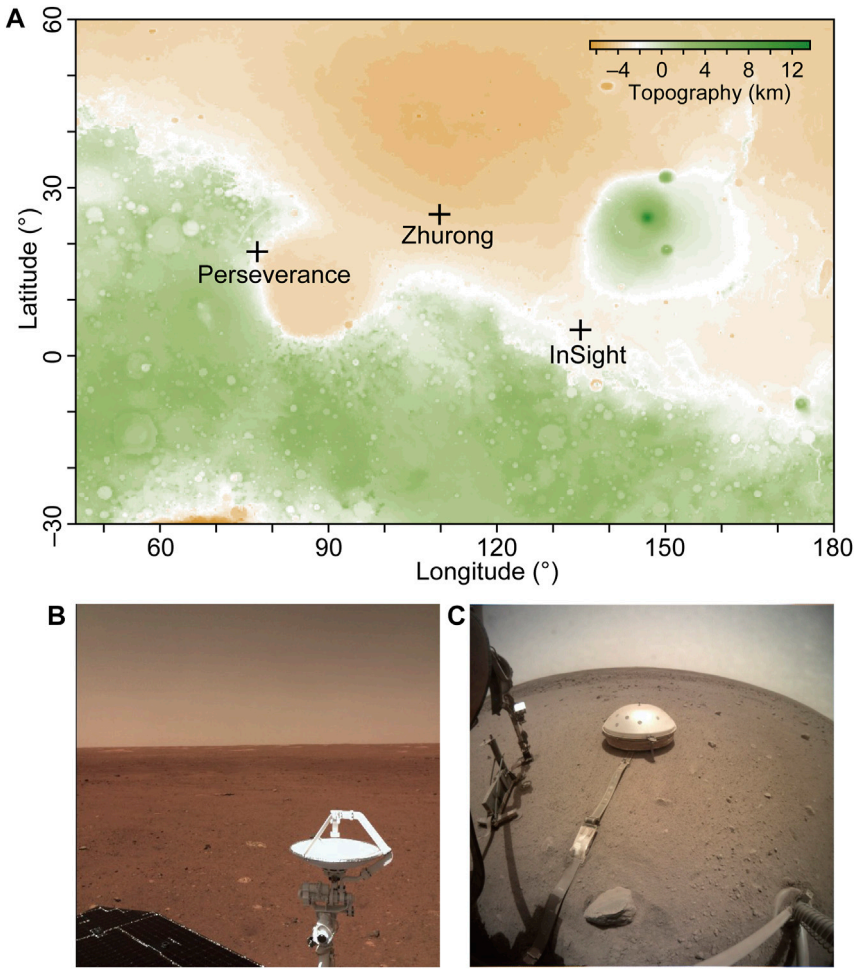

FIGURE 1
The locations of Zhurong rover, InSight lander, and Perseverance lander. **(A)** the topography around southern Utopia Planitia. **(B)** Surface view taken by navigation and terrain cameras on Zhurong rover (NaTeCam, Liang et al., 2021; Liu et al., 2021). **(C)** Surface view taken by InSight lander (https://pds-geosciences.wustl.edu/missions/insight/index.htm).

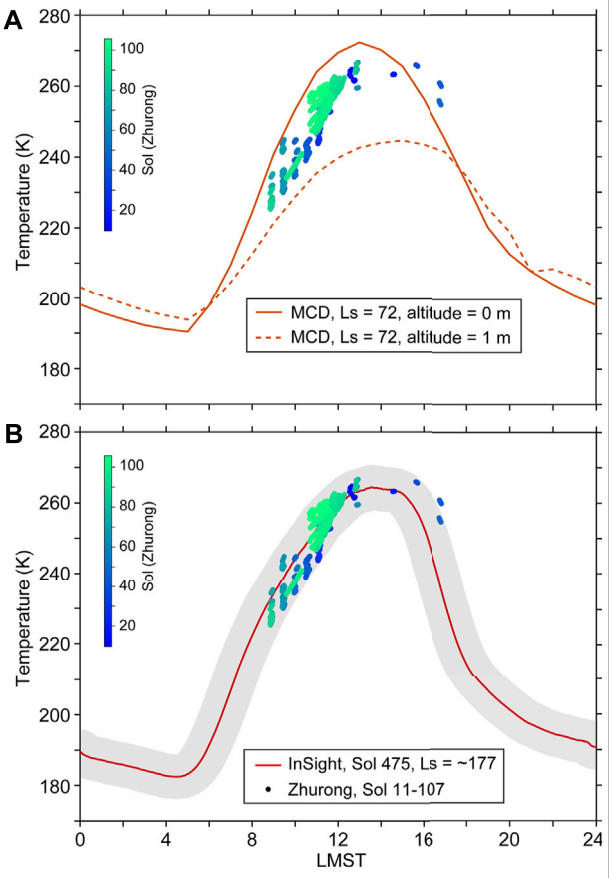

FIGURE 2
Temperature correction at the Zhurong landing site by InSight temperature observation. **(A)** Record data at the Zhurong landing site (~1 m over the ground) and MCD modeled temperature at Ls of 72° with altitudes of 0 m and 1 m, respectively. **(B)** Zhurong recorded temperature data, compared with the daily temperature records at the InSight landing site in its Sol 475, with Ls = ~177°. The gray bar indicates an error of ±8 K

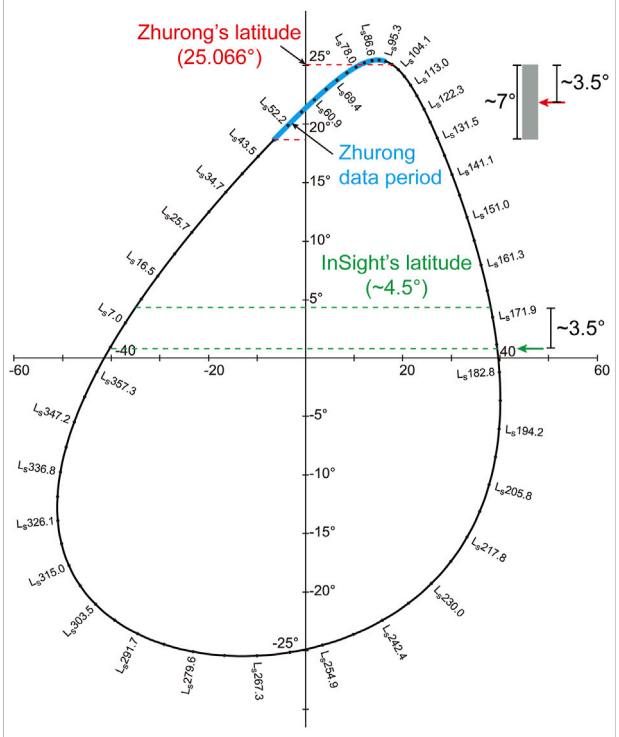

FIGURE 3
The Solar longitude (Ls) correction for the representative daily temperature at Zhurong's latitude according to InSight's latitude. The horizontal axis is the equation of time (minutes) and the vertical axis is the declination (degrees). The Zhurong landing site (at the latitude of ~25°) and InSight landing site (at the latitude of ~4.5) are marked, respectively. Zhurong temperature data period (Ls = 50–93, 72° on average) is marked as a thick blue line. The declination variation for the Zhurong data period is ~7°. For the average day (red arrow) of the Zhurong data period, there is a ~3.5-degree declination/latitude difference to its hottest day. Accordingly, a ~3.5° declination/latitude difference is applied to the InSight landing site; thus, at the InSight landing site, the day with a similar daily temperature condition to the Zhurong landing site has an Ls of ~177° (green arrow).

Mars Climate Station (MCS, Peng et al., 2020) was deployed on the deck of the Zhurong rover (Figure 1), with a height of ~1 m over the ground, to monitor air temperature, air pressure, and wind. However, the temperature monitoring only works for several short periods during the daytime; thus, the total amount of recorded temperature data is inadequate for an entire-day temperature analysis at the landing site. Fortunately, the general temperature has a high similarity within a limited spatial range, especially along a similar latitude. InSight, a Martian lander located in northern mid-low latitude like Zhurong, has collected continuous temperature data for approximately 2 martian years. InSight was equipped with Temperature and Winds for InSight (TWINS, Spiga et al., 2018), which collected continuous temperature data and thus can provide solid constraints for the reconstruction of Zhurong temperature data.

In this paper, we first reconstruct the near-surface temperature at the Zhurong landing site by incorporating the temperature data observed at the InSight lander. Then, the reconstructed near-surface data is applied to simulate the response of the subsurface of the Zhurong landing site due to the temperature changes in the air, with both daily and seasonal timescales. Finally, we discussed the possibility of the existence of water/ice according to the temperature simulation results.

Results

Temperature reconstruction of a representative day at the Zhurong landing site

As mentioned in the introduction section, during the first ~100 sols (Sol 11–Sol 107) of the Zhurong rover, only some

discrete temperature data have been collected with local mean solar time (LMST) of 09:00–17:00, basically consistent with the daily temperature modeled by MCD (Figure 2A). These discrete temperature data are not enough for a daily temperature field simulation in the subsurface under the landing site, restricting our understanding of the response of the subsurface materials due to daily and seasonal temperature changes.

Although the elevation difference between the Zhurong landing site and InSight landing site is almost 2000 m, the near-surface environment of these two sites is similar (Figures 1B,C). Therefore, we reconstruct the near-surface temperature at the Zhurong landing site by incorporating the temperature data observed at the InSight landing site according to similar solar incident conditions in an entire martian year since these two sites are both located at mid-low latitudes. Specifically, the period of Zhurong temperature data collected has average solar longitude (Ls) of 72°. At the InSight landing site, the day with similar daily temperature conditions to the Zhurong landing site has an Ls of ~177 (Figure 3). Therefore, we use the temperature data of Ls = 177° (Sol 475) at the InSight landing site as a representative day for the temperature data collecting period at Zhurong (Figure 2B). With an error bar of ±8 K (~10% of daily temperature amplitude), the representative temperature curve from InSight can cover the Zhurong data collected, indicating that the temperature reconstruction for the representative day is reasonable.

Temperature correction from the air to the ground

Although the MCD-modeled temperature can generally well cover the recorded Zhurong data (Figure 2A), the accuracy is still limited, compared with the representative temperature curve from InSight (Figure 2B). As a result, the MCD modeled temperature cannot be directly used to fit the Zhurong temperature records, nor setting the altitude as 0 m or 1 m (Figure 2A). Fortunately, the temperature ratios (ground/air) of both recorded and MCD modeled are approximately equal, according to the measured data from InSight lander and Perseverance rover (Zhang et al., 2023b). In addition, the air temperature sensors of MCS are on the deck of the Zhurong rover, ~1 m over the ground. However, the ground temperature (above the surface 0 m) is supposed to be used as the input for the simulation of heat conduction. Therefore, we correct the representative air temperature (above the surface 1 m) of Zhurong (i.e., temperature data of Ls = 177° at the InSight landing site, as reconstructed in *Temperature reconstruction of a representative day at the Zhurong landing site*) to the ground temperature (above the surface 0 m) according to the modeled air temperature and ground temperature from the MCD as below:

$$T_{0m}^{Estimated} = T_{0m}^{MCD} \frac{T_{1m,Ls=72^\circ}^{Recorded}}{T_{1m,Ls=72^\circ}^{MCD}}$$

where $T_{0m}^{Estimated}$ is the estimated ground temperature at Zhurong, which is used as the top temperature boundary for the heat conduction simulation; T_{0m}^{MCD} is the ground temperature modeled by the MCD; $T_{1m,Ls=72^\circ}^{Recorded}$ is the recorded air temperature (above the surface 1 m) corrected from InSight temperature data with Ls = 72° for Zhurong (Ls = 177° for InSight). $T_{1m,Ls=72^\circ}^{MCD}$ is the MCD-modeled air temperature (above the surface 1 m) at Zhurong. Figure 4 shows the temperature distribution through a whole year at the Zhurong landing site after above temperature correction process.

Heat conduction equation

It would be very helpful to analyze the underground structure and thermal state (temperature field) based on three-dimensional simulations. Although the previous study has revealed the structure of the subsurface under the Zhurong landing site (Li et al., 2022). However, the detailed three-dimensional structure of the shallowest 10 m remains enigmatic. Simplistically, we apply the one-dimensional version of heat conduction equation for an efficient calculation but use three sets of thermal diffusivity values to show the maximum possible range of thermal state variations.

On the near surface of Mars, the heat conduction equation can be described below (Li et al., 2022; Zhang et al., 2023b)

$$\frac{\partial T}{\partial t} = \kappa \frac{\partial^2 T}{\partial^2 z} \tag{1}$$

where T is the temperature, t is the time, z is the depth (positive downward), and κ is the thermal diffusivity of the region of interest. The solution of heat production equality generally depends on diffusion (Gläser and Gläser, 2019). At the ground surface ($z = 0$), $T_{0m}^{Estimated}$ is used as the top temperature boundary. In the heat conduction equation, T (0, t) can be written as a sine function

$$T(0,t) = T_0 + A_0 \sin\left(\frac{2\pi}{P}t + \varphi_0\right) \tag{2}$$

where P is the period (diurnal variation with P of one sol and annual variation with P of one martian year), T_0 is the average ground temperature in the period, A_0 is the amplitude, and φ_0 is the initial phase. Then the heat conduction equation can be solved as

$$T(z,t) = T_0 + \gamma z + A_0 e^{-\sqrt{\frac{\pi}{\kappa P}}z} \sin\left(\frac{2\pi}{P}t + \varphi_0 - \sqrt{\frac{\pi}{\kappa P}}z\right) \tag{3}$$

where γ is a constant to describe the thermal gradient $\partial T/\partial z$, which can be determined by Fourier's Law

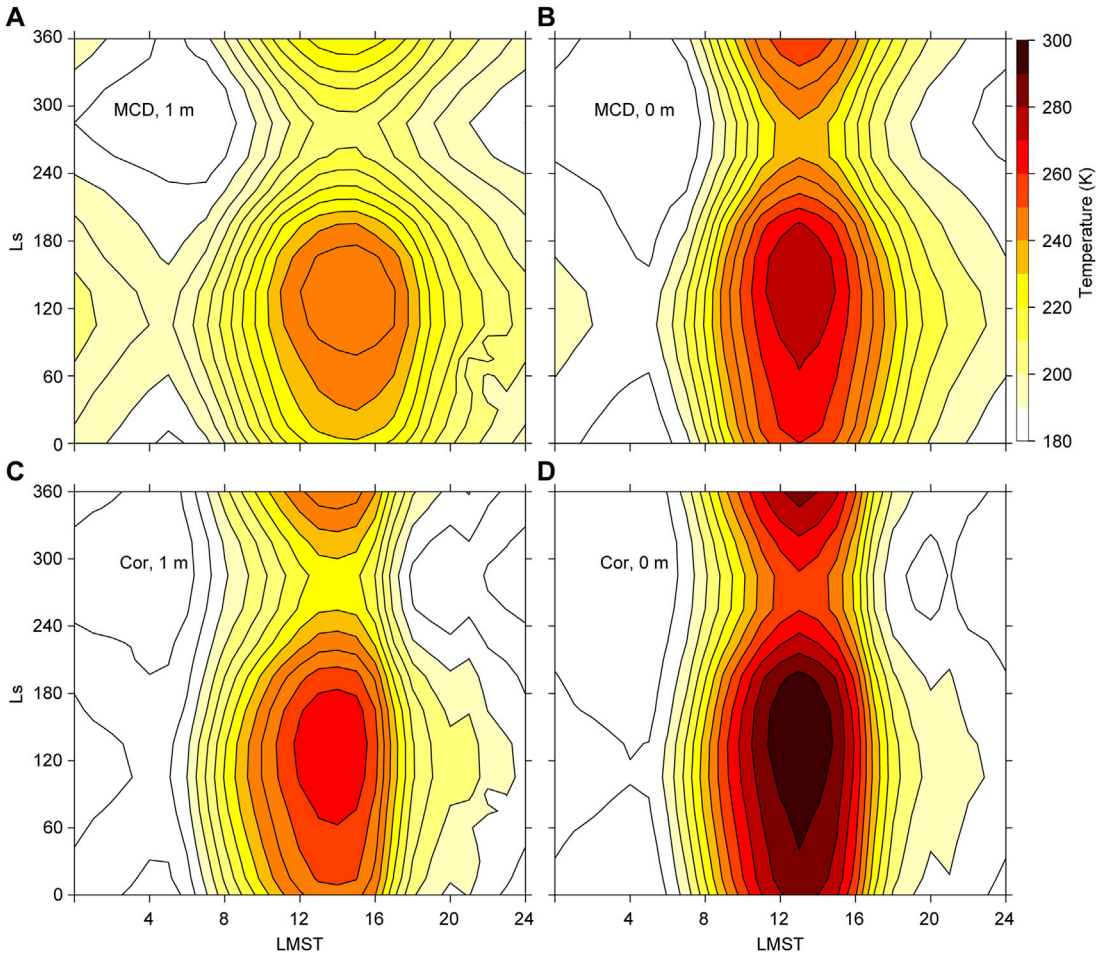

FIGURE 4
Temperature distribution through a whole year at the Zhurong landing site. **(A)** MCD modeled temperature with an altitude of 1 m (in the air); **(B)** MCD modeled temperature with an altitude of 0 m (on the ground); **(C)** InSight-based corrected temperature with an altitude of 1 m; **(D)** InSight-based corrected temperature with an altitude of 0 m.

$$\gamma = \frac{\partial T}{\partial z} = \frac{Q_0}{k_0} \tag{4}$$

where the average thermal conductivity k_0 of the Martian subsurface is set to be 0.8 $Wm^{-1}K^{-1}$ (Egea-Gonzalez et al., 2021), and the average heat flux (Q_0) of 18 mWm^{-2} is selected for the Zhurong landing site from the present-day heat flow model of Mars (Parro et al., 2017).

Figure 5 presents the diurnal temperature change in the subsurface beneath the Zhurong rover for the representative day with an average Ls of 72°. Since the *in-situ* thermal parameters have not been obtained at the Zhurong landing site, the thermal diffusivity is set as 5.1×10^{-8} (InSight measured, Spohn et al., 2018), 1×10^{-7} (water), and 1×10^{-6} (ice or sandstone, Mühll and Haeberli, 1990; Sun et al., 2016), respectively, for parameter sensitivity analysis. The simulation results show that when the thermal diffusivity is set as 5.1×10^{-8} (InSight measured) or 1×10^{-7} (water), the diurnal temperature variations over 1 K only occur within the top 30 cm (Figure 5C). Although the surface ($z = 0$) has a daily temperature variation of over 100 K, for the shallowest 8 cm, daily temperature variations are less than 25 K (Figure 5B); when the thermal diffusivity is set as ice or sandstone, the diurnal temperature variations over 1 K occur much deeper, with the depth of ~100 cm (Figure 5C). The average temperature in the top 100 cm subsurface is approximately 225 K. Without considering the heat flow from deep Mars, the temperature with depth over 100 cm is constantly ~225 K (Figure 5C). In addition, the highest temperature usually occurs at afternoon 14:00 LMST. The temperature over 273 K (melting point of water) occurs only in the shallowest several centimeters. At other times or other depths, the temperature is always less than 273 K, as low as 180 K before sunrise.

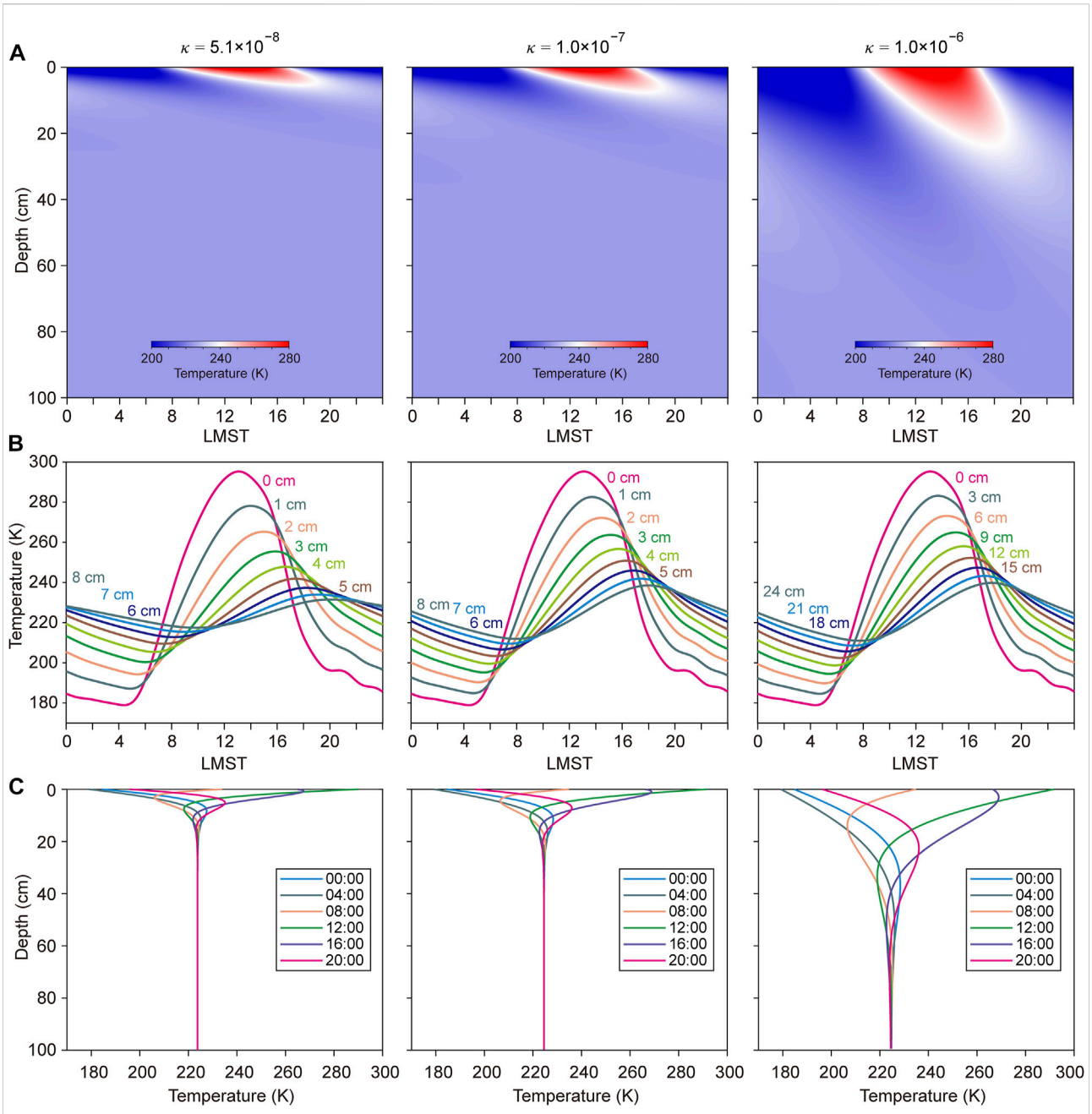

FIGURE 5
Daily temperature simulation results for the Zhurong landing site. **(A)** Daily temperature variation in the top 100 cm of the subsurface. **(B)** temperature profiles in different depths. **(C)** temperature profiles at different times of the day. The left, middle, and right columns are based on the thermal diffusivity of 5.1 × 10^{-8} (InSight measured), 1 × 10^{-7} (water), and 1 × 10^{-6} (ice or sandstone), respectively.

Seasonal variation of the subsurface temperature

Figure 6 shows the temperature profiles in Sols 11–107 of Zhurong rover (Ls of 50°–93°) at representative moments for each sol (06:00, 14:00, 18:00, and 24:00 LMST). The thermal diffusivity is also set as 5.1 × 10^{-8} (left column), 1 × 10^{-7} (middle column), and 1 × 10^{-6} (right column), respectively, for parameter sensitivity analysis. We can see that the hottest period occurs at Ls of ~90°, which is approximately the summer solstice of Zhurong landing site. In contrast, the top 100 cm temperature in spring (Ls = ~50°) is much lower.

In the subsurface of Zhurong landing site, the absence of liquid water has been investigated by radar detection, but the existence of

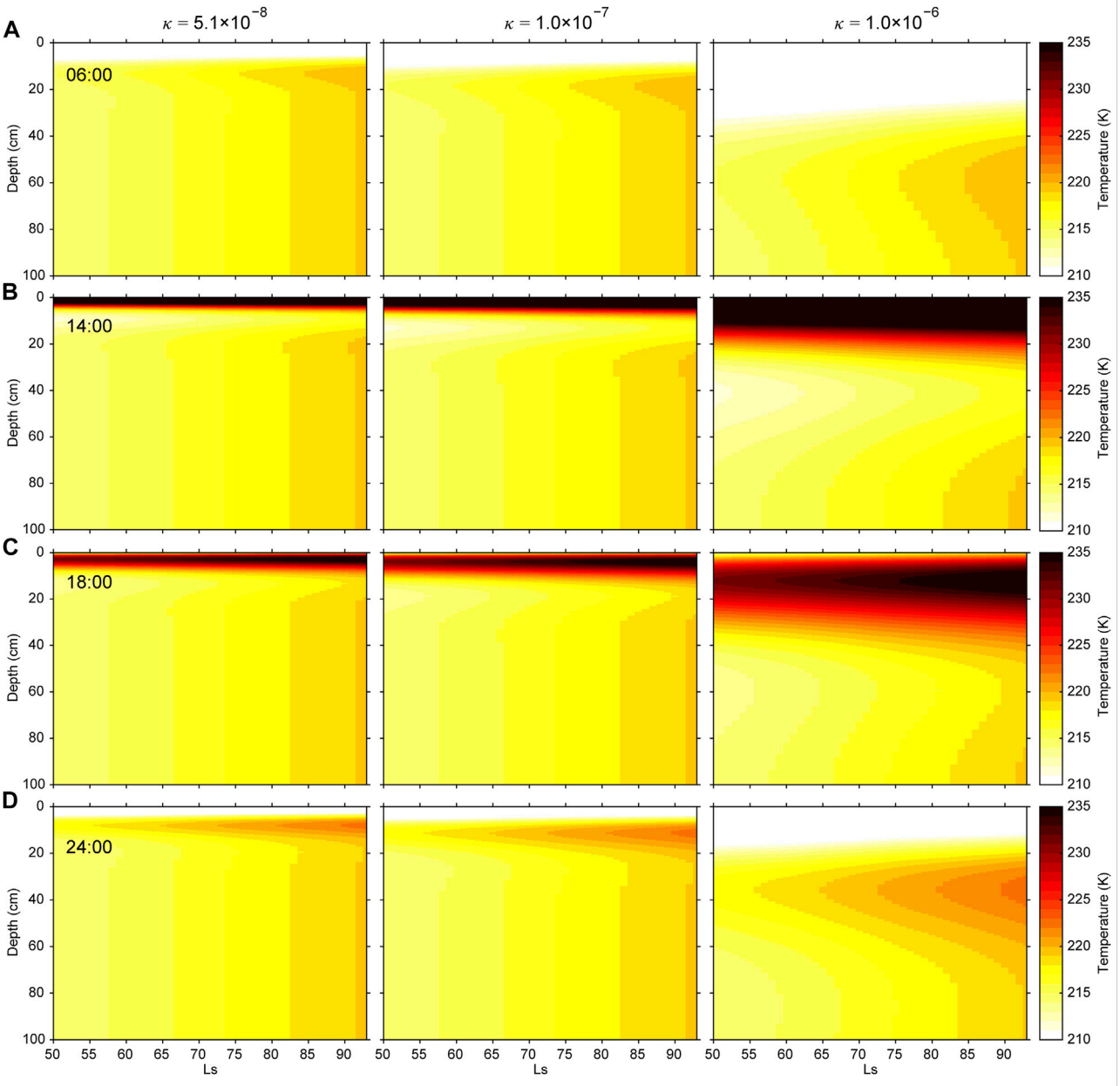

FIGURE 6
Temperature distribution in the top 100 cm subsurface under the Zhurong landing site in its Sols 11–107 with Ls of 50–93. **(A)** 06:00; **(B)** 14:00; **(C)** 18:00; **(D)** 24:00. The left, middle, and right columns are based on the thermal diffusivity of 5.1×10^{-8} (InSight measured), 1×10^{-7} (water), and 1×10^{-6} (ice or sandstone), respectively.

ice cannot be ruled out (Li et al., 2022). Taking the case with thermal diffusivity of 1×10^{-6} (right column, sand and/or stone) as an example, the temperature changes dramatically with the depth near the summer solstice, especially in the afternoon (14:00 LMST) and at sunset (18:00 LMST), which indicates the existence of multiphase in the medium if there is ice. Liquid water might exist temporarily in summer afternoons within the top ~20 cm due to ice melting if ice exists there. This simulation result shows that the best time to detect liquid water in this area might be summer afternoons (Ls = ~90, LMST = ~14:00).

Discussion and conclusion

For the temperature correction process of the Zhurong landing site according to InSight temperature observation,

although the error is only ~10% of daily temperature amplitude, the error of ±8 K is still notable (Figure 2B). In addition, the InSight-based fitting process is only according to the nighttime but without the constraints from nighttime data. As Zhurong continues to move forward on Mars, with more temperature data collected in the future (especially at nighttime), the evaluation for the near-surface daily temperature variation would be improved.

Besides the temperature boundary conditions at the top of the subsurface ($z = 0$), thermal simulation mainly relies on the thermal diffusivity of the medium. Owing to the lack of measurement for the thermal properties of the medium around the Zhurong landing site, we used three possible values in this study. In the future, thermal parameters such as thermal conductivity, thermal inertia (Mellon et al., 2000), and specific heat capacity obtained by orbital or *in-situ* observations should be incorporated into the analyses.

This paper studied the subsurface temperature in the top 100 cm of the Martian regolith, by considering several constant diffusivities. However, the density, as well as heat conductivity of the Martian regolith, likely varies with the depth, indicating that the Martian regolith shows similar properties to the lunar regolith (Hayne et al., 2017). Further work based on depth-varying property parameters should be conducted for a more realistic estimation of the temperature field in the Martian subsurface. In addition, numerical methods such as the finite-difference method (Kaczmarzyk et al., 2018) and finite-element method (Wasilewski et al., 2021) could numerically simulate the temperature field and even the thermodynamic behaviors based on a more complex and more detailed model of the subsurface. In addition, with a more detailed three-dimensional structure being detected in the future, the three-dimensional heat conduction equation can be developed to simulate a more realistic temperature field in the subsurface of Mars.

Although liquid water is most likely to appear in the afternoon of summer from the point of view of the simulated seasonal temperature variations, pressure should also be considered for evaluating the phase state of water. In the future, continuous comprehensive meteorological observations are expected to provide more data for the detection of the possible existence of water/ice on Mars. Since liquid water is believed to exist on Mars and there might have been recent aqueous activities in Utopia Planitia (Liu et al., 2022), *in-situ* detection of meteorological conditions in the polar regions would provide a valuable comparison for the detection of water/ice in the areas of Zhurong and other martian landers or rovers.

As the structure of the Martian subsurface is more clearly detected by radar in Zhurong area (Li et al., 2022), more refined thermodynamic models based on the detected structure would provide more accurate results for the temperature analysis of the subsurface in this region. For example, the modeling of both the martian regolith and the filled rocks using the finite-element method can accurately simulate the temperature distribution and its variation for the martian subsurface.

In this study, we proposed a strategy for reconstructing the near-surface temperature at the Zhurong landing site by incorporating the temperature data observed at the InSight lander. The reconstructed temperature data are then used to solve the heat equation as a boundary condition for the thermal simulation in the subsurface of the Zhurong landing site. Simulation results in both daily and annual timescales are further used to analyze the possibility of the existence of water/ice. The procedure based on a limited amount of records suggested in this study can be an example of the subsurface temperature field simulation in areas with insufficient local data, particularly on extraterrestrial objects.

Data availability statement

The Tianwen-1 data including the Mars Climate Station (MCS) data used in this study are processed and produced by the GRAS of China's Lunar and Planetary Exploration Programme and provided by CNSA at https://clpds.bao.ac.cn/web/enmanager/mars1. The TWINS datasets of InSight mission were downloaded from NASA's Planetary Data System (PDS, https://pds-geosciences.wustl.edu/missions/insight/index.htm).

Author contributions

Conceptualization: LZ and JZ; Methodology: LZ; Investigation: LZ and JZ; Visualization: LZ; Supervision: JZ; Writing—original draft: LZ and JZ; Writing—review and editing: LZ and JZ.

Funding

This research was supported by the National Natural Science Foundation of China (42204178 and 41941002), and China Postdoctoral Science Foundation 2021M703193. This research is also supported by the Key Research Program of the Chinese Academy of Sciences (ZDBS-SSWTLC001).

Acknowledgments

We thank Editor Prof. Jianguo Yan and the two reviewers for their constructive comments and suggestions, which greatly improved the clarity and readability of the manuscript. The

Supercomputing Laboratory at IGGCAS provided computing resources for the calculation in this paper.

Conflict of interest

The authors declare that the research was conducted in the absence of any commercial or financial relationships that could be construed as a potential conflict of interest.

Publisher's note

All claims expressed in this article are solely those of the authors and do not necessarily represent those of their affiliated organizations, or those of the publisher, the editors and the reviewers. Any product that may be evaluated in this article, or claim that may be made by its manufacturer, is not guaranteed or endorsed by the publisher.

References

Acuna, M. H., Connerney, J. E. P., Ness, N. F., Lin, R. P., Mitchell, D., Carlson, C. W., et al. (1999). Global distribution of crustal magnetization discovered by the Mars global surveyor MAG/ER experiment. *Science* 284, 790–793. doi:10.1126/science.284.5415.790

Banfield, D., Spiga, A., Newman, C., Forget, F., Lemmon, M., Lorenz, R., et al. (2020). The atmosphere of Mars as observed by InSight. *Nat. Geosci.* 13 (3), 190–198. doi:10.1038/s41561-020-0534-0

Charalambous, C., Stott, A. E., Pike, W. T., McClean, J. B., Warren, T., Spiga, A., et al. (2021). A comodulation analysis of atmospheric energy injection into the ground motion at InSight, Mars. *JGR. Planets* 126 (4), e2020JE006538. doi:10.1029/2020JE006538

Christensen, U. R., Holzwarth, V., and Reiners, A. (2009). Energy flux determines magnetic field strength of planets and stars. *Nature* 457, 167–169. doi:10.1038/nature07626

Egea-Gonzalez, I., iménez-Díaz, A., Parro, L. M., Mansilla, F., Holmes, J. A., Lewis, S. R., et al. (2021). Regional heat flow and subsurface temperature patterns at Elysium Planitia and Oxia Planum areas, Mars. *Icarus* 353, 113379. doi:10.1016/j.icarus.2019.07.013

Forget, F., Hourdin, F., Fournier, R., Hourdin, C., Talagrand, O., Collins, M., et al. (1999). Improved general circulation models of the Martian atmosphere from the surface to above 80 km. *J. Geophys. Res.* 104 (E10), 24155–24175. doi:10.1029/1999JE001025

Gläser, P., and Gläser, D. (2019). Modeling near-surface temperatures of airless bodies with application to the Moon. *Astron. Astrophys.* 627, A129. doi:10.1051/0004-6361/201935514

Gou, S., Yue, Z., Di, K., Zhao, C., Bugiolacchi, R., Xiao, J., et al. (2022). Transverse aeolian ridges in the landing area of the Tianwen-1 Zhurong rover on Utopia Planitia, Mars. *Earth Planet. Sci. Lett.* 595, 117764. doi:10.1016/j.epsl.2022.117764

Hayne, P. O., Bandfield, J. L., Siegler, M. A., Vasavada, A. R., Ghent, R. R., Williams, J. P., et al. (2017). Global regolith thermophysical properties of the moon from the diviner lunar radiometer experiment. *J. Geophys. Res. Planets* 122, 2371–2400. doi:10.1002/2017JE005387

Kaczmarzyk, M., Gawronski, M., and Piatkowski, G. (2018). Application of Finite Difference Method for determining lunar regolith diurnal temperature distribution. *E3S Web Conf.* 49, 00052. doi:10.1051/e3sconf/20184900052

Li, C., Zheng, Y., Wang, X., Zhang, J., Wang, Y., Chen, L., et al. (2022). Layered subsurface in Utopia Basin of Mars revealed by Zhurong rover radar. *Nature* 610, 308–312. doi:10.1038/s41586-022-05147-5

Liang, X., Chen, W., Cao, Z., Wu, F., Lyu, W., Song, Y., et al. (2021). The navigation and terrain cameras on the Tianwen-1 Mars rover. *Space Sci. Rev.* 217 (3), 37–20. doi:10.1007/s11214-021-00813-y

Liu, J., Li, C., Zhang, R., Rao, W., Cui, X., Geng, Y., et al. (2021). Geomorphic contexts and science focus of the Zhurong landing site on Mars. *Nat. Astron.* 6 (1), 65–71. doi:10.1038/s41550-021-01519-5

Liu, Y., Wu, X., Zhao, Y. S., Pan, L., Wang, C., Liu, J., et al. (2022). Zhurong reveals recent aqueous activities in Utopia Planitia, Mars. *Sci. Adv.* 8 (19), eabn8555. doi:10.1126/sciadv.abn8555

Mellon, M. T., Jakosky, B. M., Kieffer, H. H., and Christensen, P. R. (2000). High-resolution thermal inertia mapping from the Mars global surveyor thermal emission spectrometer. *Icarus* 148 (2), 437–455. doi:10.1006/icar.2000.6503

Mühll, D. V., and Haeberli, W. (1990). Thermal characteristics of the permafrost within an active rock glacier (Murtèl/Corvatsch, Grisons, Swiss Alps). *J. Glaciol.* 36 (123), 151–158. doi:10.3189/S0022143000009382

Niu, S., Zhang, F., Di, K., Gou, S., and Yue, Z. (2022). Layered ejecta craters in the candidate landing areas of China's first Mars mission (Tianwen-1): Implications for subsurface volatile concentrations. *JGR. Planets* 127 (3), e2021JE007089. doi:10.1029/2021JE007089

Parro, L. M., Jiménez-Díaz, A., Mansilla, F., and Ruiz, J. (2017). Present-day heat flow model of Mars. *Sci. Rep.* 7 (1), 45629–9. doi:10.1038/srep45629

Peng, Y., Zhang, L., Cai, Z., Wang, Z., Jiao, H., Wang, D., et al. (2020). Overview of the Mars climate station for Tianwen-1 mission. *Earth Planet. Phys.* 4 (4), 371–383. doi:10.26464/epp2020057

Spiga, A., Banfield, D., Teanby, N. A., Forget, F., Lucas, A., Kenda, B., et al. (2018). Atmospheric science with InSight. *Space Sci. Rev.* 214 (7), 109–164. doi:10.1007/s11214-018-0543-0

Spohn, T., Grott, M., Smrekar, S. E., Knollenberg, J., Hudson, T. L., Krause, C., et al. (2018). The heat flow and physical properties package (HP^3) for the InSight mission. *Space Sci. Rev.* 214 (5), 96–33. doi:10.1007/s11214-018-0531-4

Stanley, S., Elkins-Tanton, L., Zuber, M. T., and Parmentier, E. M. (2008). Mars' paleomagnetic field as the result of a single-hemisphere dynamo. *Science* 321, 1822–1825. doi:10.1126/science.1161119

Sun, Q., Lü, C., Cao, L., Li, W., Geng, J., and Zhang, W. (2016). Thermal properties of sandstone after treatment at high temperature. *Int. J. Rock Mech. Min. Sci.* 85, 60–66. doi:10.1016/j.ijrmms.2016.03.006

Wasilewski, T. G., Barciński, T., and Marchewka, M. (2021). Experimental investigations of thermal properties of icy lunar regolith and their influence on phase change interface movement. *Planet. Space Sci.* 200, 105197. doi:10.1016/j.pss.2021.105197

Wu, X., Liu, Y., Zhang, C., Wu, Y., Zhang, F., Du, J., et al. (2021). Geological characteristics of China's Tianwen-1 landing site at Utopia Planitia, Mars. *Icarus* 370, 114657. doi:10.1016/j.icarus.2021.114657

Ye, B., Qian, Y., Xiao, L., Michalski, J. R., Li, Y., Wu, B., et al. (2021). Geomorphologic exploration targets at the Zhurong landing site in the southern Utopia Planitia of Mars. *Earth Planet. Sci. Lett.* 576, 117199. doi:10.1016/j.epsl.2021.117199

Zhang, L., Gao, F., Liu, Z., Cao, P., and Zhang, J. (2023a). Temperature-dependent modal analysis of InSight lander on Mars. *Geophysics* 88 (2). doi:10.1190/geo2022-0272.1

Zhang, L., Zhang, J., Mitchell, R. N., Cao, P., and Liu, J. (2023b). A thermal origin for super-high-frequency marsquakes. *Icarus* 115327, 115327. doi:10.1016/j.icarus.2022.115327

Zhang, L., Zhang, J., and Mitchell, R. N. (2022a). Dichotomy in crustal melting on early Mars inferred from antipodal effect. *Innovation* 3 (5), 100280. doi:10.1016/j.xinn.2022.100280

Zhao, J., Xiao, Z., Huang, J., Head, J. W., Wang, J., Shi, Y., et al. (2021). Geological characteristics and targets of high scientific interest in the Zhurong landing region on Mars. *Geophys. Res. Lett.* 48 (20), e2021GL094903. doi:10.1029/2021GL094903

Zhong, S., and Zuber, M. T. (2001). Degree-1 mantle convection and the crustal dichotomy on Mars. *Earth Planet. Sci. Lett.* 189, 75–84. doi:10.1016/S0012-821X(01)00345-4

Zhou, B., Shen, S., Lu, W., Liu, Q., Tang, C., Li, S., et al. (2020). The Mars rover subsurface penetrating radar onboard China's Mars 2020 mission. *Earth Planet. Phys.* 4 (4), 1–10. doi:10.26464/epp2020054